Varicose dynamics of liquid curtain: Linear analysis and volume-of-fluid simulations

Alessandro Della Pia*
Scuola Superiore Meridionale, School for Advanced Studies, Naples 80128, Italy

Matteo Chiatto and Luigi de Luca
Department of Industrial Engineering, University of Naples "Federico II", Naples 80125, Italy

(Received 5 December 2023; accepted 23 July 2024; published 9 August 2024)

The varicose dynamics of a forced gravitational liquid sheet (curtain) issuing into a quiescent gaseous ambient is numerically investigated in this work. The study is relevant for technological applications such as coating deposition, where varicose perturbations of the curtain interfaces can arise due to axial velocity fluctuations coming from the delivering pump placed upstream of the coating die. The investigation is performed in supercritical regime, namely, for Weber number We > 1. Two methodologies are employed: a simplified one-dimensional (1D) linear model and two-dimensional (2D) volume-of-fluid simulations. Using harmonic forcing perturbations of the streamwise velocity applied at the inlet section, the curtain varicose dynamics is excited by varying the forcing frequency f and amplitude A_u of the perturbations for different values of We. As a significant result, the 1D analysis reveals that the curtain oscillations amplitude reaches a maximum value for a certain forcing frequency $f = f_{\max}$. In other terms, it is found that the flow manifests a resonance behavior, with the oscillation frequency $f_{\max}$ and corresponding amplitude $A_{h,\max}$ both scaling as $\mathrm{We}^{1/3}$, while the average wavelength $\bar{\lambda}_{\max}$ scales as $\mathrm{We}^{-1/3}$. These scaling laws are confirmed both by theoretical insights and 2D simulations. Moreover, it is found that the 2D curtain breaks up numerically by increasing the forcing amplitude A_u. The numerical rupture is determined by a progressive curtain thinning induced by the varicose deformation, which moves upstream by increasing We, i.e., downstream by increasing the surface tension coefficient. In this respect, surface tension is found to play a stabilizing role on the varicose oscillations of the curtain.

DOI: 10.1103/PhysRevFluids.9.084003

I. INTRODUCTION

The stability and dynamics of gravitational liquid sheets (curtains) interacting with an initially quiescent gaseous ambient have been investigated by the scientific community for decades (Lin [1]).

Within a linear mathematical framework, Rayleigh [2] showed two linearly independent wave modes of a liquid sheet, namely, sinuous and varicose modes, which were then experimentally observed by Taylor [3]. The sinuous mode moves the two free surfaces of the curtain in phase, while the varicose one symmetrically moves the free surfaces in opposite directions (see Fig. 1 in the following Sec. II). First, investigations of the stability of sinuous and varicose modes were performed by Squire [4] through a classic temporal linear stability approach. For finite values of the gas-to-liquid density ratio r_ρ, the theory predicted instability of sinuous modes only for Weber number values greater than 1. The definition of the Weber number here employed is

*Contact author: alessandro.dellapia@unina.it

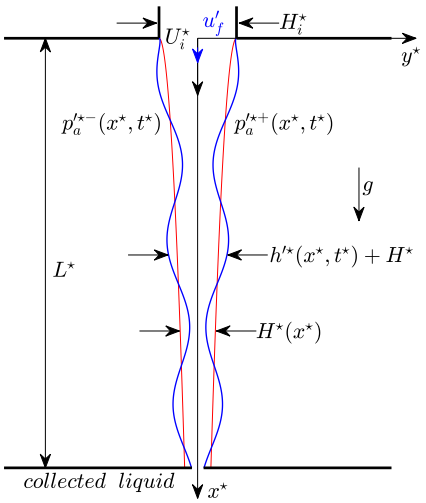

FIG. 1. Sketch of the gravitational liquid sheet (curtain) flow. The forcing term u'_f superposed to the base flow (red lines) excites the varicose deformation of the curtain shape (blue lines).

$\mathrm{We} = \rho_l U_i^{\star 2} H_i^\star/(2\sigma)$, where ρ_l is the liquid density, $U_i^\star$ and $H_i^\star$ are the inlet velocity and thickness of the sheet, respectively, and σ the surface tension coefficient.

The experimental evidence contradicted the theoretical result by Squire [4] a few years later. The experiments performed by Brown [5] indicated instability for $\mathrm{We} < 1$ in the form of expanding holes within the curtain, eventually determining its breakup. More recently, Roche *et al.* [6] also observed ruptures in falling sheets with $\mathrm{We} < 1$, which subsequently returned to a stable state, while Le Grand-Piteira *et al.* [7] reported falling sheets able to withstand relatively high amplitude sinuous oscillations without rupture.

To improve the agreement between the experimental evidence and theoretical predictions of the curtain dynamics, a local spatiotemporal stability approach based on the method by Bers [8] was employed first by Lin *et al.* [9] and then by de Luca and Costa [10], who considered a slightly nonparallel (gravitational) base flow. The former work predicted neutral stability for sinuous disturbances in a liquid sheet when $\mathrm{We} < 1$ and $r_\rho = 0$. The latter work predicted stable sinuous disturbances when $\mathrm{We} > 1$ and $r_\rho = 0$, and absolutely unstable sinuous disturbances when $\mathrm{We} < 1$ and $r_\rho = 0$, supporting the findings of Brown [5]. More recently, Barlow *et al.* [11] showed that, if perturbed both in velocity and position, subcritical plane liquid sheets ($\mathrm{We} < 1$) reveal absolute instability, with algebraic temporal growth of sinuous modes following the power law $t^{1/3}$, as first predicted by de Luca and Costa [10].

The possibility to perform both direct numerical simulations and modal decompositions of the relevant two-phase flow has recently disclosed new aspects of liquid sheets unsteady dynamics, both in supercritical ($\mathrm{We} > 1$) and subcritical ($\mathrm{We} < 1$) regimes.

A linear destabilization mechanism of sinuous modes based on the interaction between the liquid phase and the surrounding gaseous environment has been detected in supercritical conditions by Della Pia *et al.* [12], who derived the eigenvalues spectrum of the one-dimensional curtain flow and showed it is unstable when the density ratio r_ρ exceeds a threshold value. This result was confirmed by Colanera *et al.* [13], who derived the BiGlobal spectrum of the curtain flow by performing a dynamic mode decomposition analysis based on two-dimensional nonlinear simulation data.

The sinuous forced dynamics has also been recently studied by Torsey *et al.* [14], who considered an infinite curtain subjected to sinusoidal ambient pressure disturbances not coupled with the curtain motion, and by Chiatto and Della Pia [15], who employed a theoretical model accounting for the finite length of the curtain and a sheet-ambient interaction term. Moreover, the latter authors found

a strict agreement between experimental values of the natural oscillation frequency of the curtain and linear stability analysis predictions based on an inviscid one-dimensional model. In particular, an abrupt increase (jump) in the natural frequency at the transcritical threshold (We = 1) was found both in experiments and theoretical predictions. Note that the occurrence of the frequency jump was also theoretically predicted by Girfoglio *et al.* [16], who studied a liquid curtain confined by an air cushion located on one side of the sheet, namely, the nappe flow configuration, which has also been recently simulated using the volume-of-fluid technique by Bodhanwalla *et al.* [17].

For We $<$ 1, an energy budget decomposition analysis of the curtain flow recently performed by Della Pia *et al.* [18] identified surface tension as a possible physical mechanism responsible for the sinuous modes instability in subcritical conditions, as the Weber number is progressively decreased down to $\mathrm{We_{th}}$. The threshold Weber number $\mathrm{We_{th}}$ was defined as the We value for which the sheet is entirely subcritical (local Weber number less than unity everywhere along the curtain). In these conditions, a transient algebraic growth of perturbations was found in both asymptotically stable ($\mathrm{We_{th}} < \mathrm{We} < 1$) and unstable ($\mathrm{We} < \mathrm{We_{th}}$) regimes, thus retrieving previous results by de Luca and Costa [10] and Barlow *et al.* [11].

From the literature review summarized above, it arises that the sinuous dynamics of gravitational liquid sheets has been deeply investigated over the years by means of theoretical, numerical, and experimental approaches, both for We $>$ 1 and We $<$ 1. On the contrary, a corresponding systematic characterization of the varicose dynamics of this class of flows still needs to be improved in the literature. On the one hand, the topic is particularly relevant for industrial processes such as coating deposition (Weinstein and Ruschak [19]). In this application, it is fundamental to maintain the curtain stable during the whole process. Varicose perturbations of the curtain interfaces can arise due to fluctuations of the streamwise velocity component coming from the liquid pump, which is placed upstream of the coating die used to deliver the fluid and to form the curtain. On the other hand, it has been recently shown that varicose modes can arise in sinuously forced curtain flow configurations in resonance conditions, giving rise to a nonlinear sinuous-varicose modes interaction in two-dimensional direct numerical simulations (Della Pia *et al.* [20]; Colanera *et al.* [21]). In order to identify the physical mechanisms responsible for the excitation of the varicose modes in such scenarios, a weakly nonlinear mathematical model of the curtain dynamics should be developed, whose predictions could be finally compared with results coming from the linear analysis of the sinuous and varicose modes evolution.

Therefore, as a further step towards the derivation of a weakly nonlinear mathematical model accounting for the coupling between sinuous and varicose modes in the curtain flow, this work aims to provide a numerical characterization of the varicose dynamics of a gravitational liquid sheet, which is excited by harmonic disturbances of the inlet streamwise velocity component u. The investigation is performed in a supercritical regime (We $>$ 1) through a simplified one-dimensional linear model (Sec. II A) and two-dimensional volume-of-fluid simulations (Sec. II B). The first results are shown in Sec. III, where the varicose dynamics is explored by varying the forcing frequency f and the Weber number We, thus identifying different flow conditions depending on the specific values of the two parameters. Afterwards, the effect of the forcing amplitude A_u is investigated in Sec. IV, focusing attention on the most relevant flow conditions outlined in the first part of the analysis. Conclusions are finally drawn in Sec. V.

II. PHYSICAL LAYOUT AND METHODOLOGIES

The gravitational liquid sheet (curtain) flow here considered is schematically reported in Fig. 1. In the unperturbed configuration, the curtain issues vertically (along the $x^\star$ direction) into a quiescent gaseous ambient, and it is characterized by a steady velocity distribution and two symmetrical free interfaces (red lines in Fig. 1). Due to the gravitational acceleration g, the unperturbed thickness distribution $H^\star$ decreases by moving downstream along $x^\star$. A streamwise velocity perturbation u'_f is introduced at the inlet section ($x^\star = 0$) and excites the sheet unsteady dynamics, which is characterized by a varicose (i.e., symmetric with respect to $x^\star$) displacement of the right ($y^{\star+}$) and

left ($y^{\star -}$) interfaces (blue lines in Fig. 1). The total thickness distribution $h^\star(x^\star, t^\star)$ thus results in the sum of the base flow $H^\star(x^\star)$ and the induced perturbation $h'^\star(x^\star, t^\star)$. In terms of the curtain interfaces positions, it is given as

$$h^\star(x^\star, t^\star) = y^{\star +}(x^\star, t^\star) - y^{\star -}(x^\star, t^\star). \tag{1}$$

A. One-dimensional linear modeling

Starting from the two-dimensional Euler equations closed by kinematic and dynamic conditions imposed at the free interfaces, a simplified inviscid model of the varicose curtain dynamics is hereafter derived.

The simplifying assumptions are the same as those made by Della Pia *et al.* [12] to study the sinuous dynamics of this class of flows. The unperturbed curtain configuration is assumed to be thin with respect to the wavelength of superposed disturbances, so that velocity profiles can be considered locally uniform across the sheet thickness (one-dimensional flow assumption). The generic unsteady quantity, $\phi^\star$, is considered as the sum of a steady contribution and a perturbation, $\phi^\star = \Phi^\star + \phi'^\star$. Note that the apex $\star$ denotes, here as elsewhere, dimensional quantities. Within the approximation of small perturbations, the mass and $x^\star$-momentum balances are formulated by neglecting the products of perturbation terms (linear flow assumption) and then integrated along $y^\star$, and read as

$$\frac{\partial h'^\star}{\partial t^\star} = -\frac{\partial}{\partial x^\star}(U^\star h'^\star + H^\star u'^\star), \tag{2}$$

$$\frac{\partial u'^\star}{\partial t^\star} + \frac{\partial}{\partial x^\star}(U^\star u'^\star) = \frac{\sigma}{2\rho_l}\frac{\partial^3 h'^\star}{\partial x^{\star 3}} - \frac{1}{2\rho_l}\frac{\partial (p_a'^{\star +} + p_a'^{\star -})}{\partial x^\star}, \tag{3}$$

being

$$p_a'^{\star +} + p_a'^{\star -} = -\frac{\rho_a}{\pi}\int_0^{L^\star} \frac{\partial^2 h'^\star}{\partial t^{\star 2}} \ln\left|\frac{x^\star - \xi^\star}{L^\star}\right| d\xi^\star. \tag{4}$$

In Eqs. (2) and (3), $H^\star$ and $U^\star$ are the base flow thickness and velocity distributions, respectively, while $h'^\star$ and $u'^\star$ are the corresponding perturbations. Moreover, $L^\star$ is the curtain length; ρ_l, ρ_a, and σ stand for the liquid density, the gaseous ambient density, and the surface tension coefficient, respectively; and $t^\star$ denotes the time. In Eq. (4), the ambient pressure perturbations of the right ($p_a'^{\star +}$) and left ($p_a'^{\star -}$) curtain-ambient interfaces are respectively given as

$$p_a'^{\star +} = -\frac{\rho_a}{\pi}\int_0^{L^\star} \frac{\partial^2 y'^{\star +}}{\partial t^{\star 2}} \ln\left|\frac{x^\star - \xi^\star}{L^\star}\right| d\xi^\star, \tag{5}$$

$$p_a'^{\star -} = \frac{\rho_a}{\pi}\int_0^{L^\star} \frac{\partial^2 y'^{\star -}}{\partial t^{\star 2}} \ln\left|\frac{x^\star - \xi^\star}{L^\star}\right| d\xi^\star, \tag{6}$$

which are derived by employing the unsteady Bernoulli's equation in the absence of external gas velocity (see Kornecki *et al.* [22] and Chap. 5 of De Rosa [23] for further details). Note that the symbol $\xi^\star$ in Eqs. (5) and (6) denotes the spatial integration variable, which spans the entire liquid sheet length $L^\star$. The curtain and gaseous ambient dynamics are thus coupled through the integral term represented by Eq. (4), being the local ambient pressure perturbations dependent on the global liquid sheet deformation.

The dimensionless form of Eqs. (2) and (3) is finally obtained:

$$\frac{\partial h'}{\partial t} + U\frac{\partial h'}{\partial x} = -\frac{\varepsilon}{U}\frac{\partial u'}{\partial x} - h'\frac{\partial U}{\partial x} + \frac{\varepsilon u'}{U^2}\frac{\partial U}{\partial x}, \tag{7}$$

$$\frac{\partial u'}{\partial t} + U\frac{\partial u'}{\partial x} = -u'\frac{\partial U}{\partial x} + \frac{\varepsilon}{4We}\frac{\partial^3 h'}{\partial x^3} + \frac{r_\rho}{2\pi}\frac{\partial}{\partial x}\int_0^1 \frac{\partial^2 h'}{\partial t^2}\ln|x-\xi|\,d\xi, \tag{8}$$

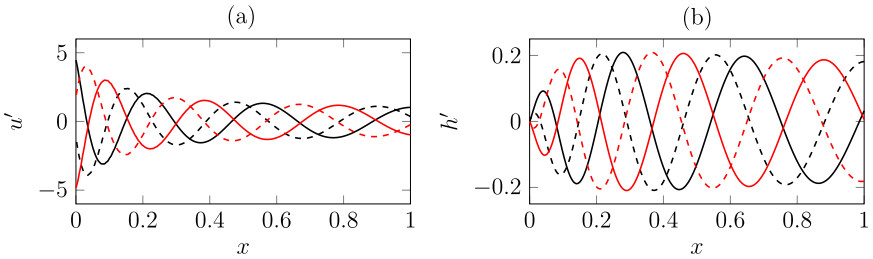

FIG. 2. One-dimensional velocity u' (a) and thickness h' (b) streamwise distributions at different fractions of an oscillation period $T = 1/f$: $t = 0T$ (black dashed curve); $0.25T$ (black continuous curve); $0.5T$ (red dashed curve); $0.75T$ (red continuous curve). Here, We $= 2.5$, $A_u = 0.1$, and $f = 5.34$.

where Eq. (4) has been substituted in Eq. (3), and the following dimensionless parameters,

$$\mathrm{We} = \frac{\rho_l U_i^{\star 2} H_i^\star}{2\sigma}, \quad \mathrm{Fr} = \frac{U_i^{\star 2}}{gL^\star}, \quad \varepsilon = \frac{H_i^\star}{L^\star}, \quad r_\rho = \frac{\rho_a}{\rho_l}, \tag{9}$$

and nondimensional variables,

$$H = \frac{H^\star}{H_i^\star}, \quad U = \frac{U^\star}{U_i^\star}, \quad h' = \frac{h'^\star}{H_i^\star}, \quad u' = \frac{u'^\star}{\varepsilon U_i^\star}, \quad x = \frac{x^\star}{L^\star}, \quad t = \frac{t^\star U_i^\star}{L^\star}, \tag{10}$$

have been introduced. In Eq. (9), We is the Weber number, Fr the Froude number, ε the curtain slenderness ratio, and r_ρ the density ratio. Based on the works by Finnicum *et al.* [24] and Weinstein *et al.* [25], the Torricelli's free-fall model,

$$U = \sqrt{1 + \frac{2}{\mathrm{Fr}} x}, \tag{11}$$

is employed as the base flow in Eqs. (7) and (8).

The two unknowns in Eqs. (7) and (8) are the spatiotemporal evolutions of the curtain thickness $[h'(x,t)]$ and velocity $[u'(x,t)]$ perturbations. The system (7)-(8) is thus closed by assigning the following inlet boundary conditions,

$$h'(0,t) = 0, \tag{12}$$

$$u'(0,t) = u'_f = \frac{A_u}{\varepsilon} \sin(2\pi f t), \tag{13}$$

the free-outflow condition at the outlet section ($x = 1$) being self-guaranteed. The coefficients $A_u = A_u^\star / U_i^\star$ and $f = f^\star L^\star / U_i^\star$ in Eq. (13) represent the amplitude and frequency of the harmonic forcing, respectively. As will be shown in Sec. III, adding the forcing perturbation [Eq. (13)] allows one to identify the natural frequencies of the varicose dynamics by searching for the resonance conditions of the curtain flow.

The numerical resolution of the system (7)-(8) equipped with boundary conditions (12) and (13) is performed by means of a standard finite-difference discretization method in MATLAB. Note that, for any $x = \xi$, the integrand in Eq. (8) is singular, and its evaluation requires a suitable treatment (De Rosa [23]).

A typical one-dimensional curtain flow unsteady solution obtained employing the procedure described above is provided in Fig. 2, where the velocity u' [panel (a)] and thickness h' [panel (b)] streamwise distributions are reported at different fractions of the oscillation period $T = 1/f$. The numerical solutions shown in Fig. 2 are evaluated for the following values of the governing parameters [previously defined in Eq. (9)]: We $= 2.5$, Fr $= 0.33$, $\varepsilon = 0.02$, and $r_\rho = 0.01$. Moreover, the forcing amplitude and frequency are chosen equal to $A_u = 0.1$ and $f = 5.34$, respectively (further

discussion will be provided in Sec. III). The analysis of Fig. 2 reveals that the oscillatory velocity perturbation u'_f introduced at the inlet [Eq. (13)] yields an analogous perturbation of the curtain thickness, which results in a traveling wave advected downstream towards the curtain tail region by the underlying base flow U [Eq. (11)]. For We $= 2.5$, the maximum temporal oscillations amplitude of the thickness distribution $h'(x)$ over x is equal to $A_h = 0.21$ [see Fig. 2(b)]. Note that de Luca and Costa [10] also found, by means of a spatiotemporal linear stability analysis approach, that for density ratio $r_\rho > 0$, the varicose modes of a curtain are convectively unstable, and so perturbations travel downstream by leaving the liquid sheet globally stable.

The effect of the forcing frequency f on the spatiotemporal curtain dynamics $h'(x, t)$ at different values of the Weber number We will be investigated in Sec. III.

B. Two-dimensional volume-of-fluid simulations

The two-dimensional two-phase flow field represented by the liquid curtain interacting with the initially quiescent gaseous environment is modeled through the one-fluid formulation of incompressible Navier-Stokes equations (Scardovelli and Zaleski [26]), reading as

$$\frac{\partial u_i^\star}{\partial x_i^\star} = 0, \tag{14a}$$

$$\rho\left(\frac{\partial u_i^\star}{\partial t^\star} + u_j^\star \frac{\partial u_i^\star}{\partial x_j^\star}\right) = -\frac{\partial p^\star}{\partial x_i^\star} + \rho g_i + \frac{\partial}{\partial x_j^\star}\left[\mu\left(\frac{\partial u_i^\star}{\partial x_j^\star} + \frac{\partial u_j^\star}{\partial x_i^\star}\right)\right] + \sigma\kappa^\star n_i \delta_S, \tag{14b}$$

$$\frac{\partial C}{\partial t^\star} + \frac{\partial C u_i^\star}{\partial x_i^\star} = 0. \tag{14c}$$

The vectors $\mathbf{u}^\star = (u^\star, v^\star)$ and $\mathbf{g} = (g, 0)$ represent the flow velocity and the gravitational acceleration, respectively, $p^\star$ the pressure field, $\kappa^\star$ the mean gas-liquid interface curvature, and $\mathbf{n} = (n_x, n_y)$ the outward pointing normal vector to the interface. The Dirac distribution function δ_S is equal to 1 at the interface, and 0 elsewhere. The density ρ and viscosity μ fields are discontinuous across the interface separating the two fluids,

$$\rho = \rho_a + (\rho_l - \rho_a)C, \tag{15a}$$

$$\mu = \mu_a + (\mu_l - \mu_a)C, \tag{15b}$$

being the volume fraction C a discontinuous function, which is equal to either 1 or 0 in the liquid or gaseous regions, respectively.

Equations (14a)–(14c) are solved using the finite volume method in the open-source code BASILISK, an improved version of GERRIS (Popinet [27]) that has been extensively used and validated for plane liquid jet flow problems (Schmidt and Oberleithner [28]; Schmidt *et al.* [29]; Della Pia *et al.* [20]). The code employs the volume-of-fluid (VOF) method by Scardovelli and Zaleski [26] to track the interface on a quadtree structured grid, with an adaptive mesh refinement based on a criterion of wavelet-estimated discretization error (van Hooft *et al.* [30]) and no special treatment required in the presence of liquid phase breakup (Agbaglah [31]). A multigrid solver is employed to satisfy the incompressibility condition, while the calculation of the surface tension term is based on the balanced continuum surface force technique (Francois *et al.* [32]), which is coupled with a height-function curvature estimation method to avoid the generation of spurious currents. For exhaustive details about the code BASILISK, the reader is referred to Popinet [27,33] and to the software official website [34,35].

The computational domain employed to calculate two-dimensional curtain flow solutions is a square, whose length side is equal to the curtain length $L^\star$. The liquid sheet shape is initialized as

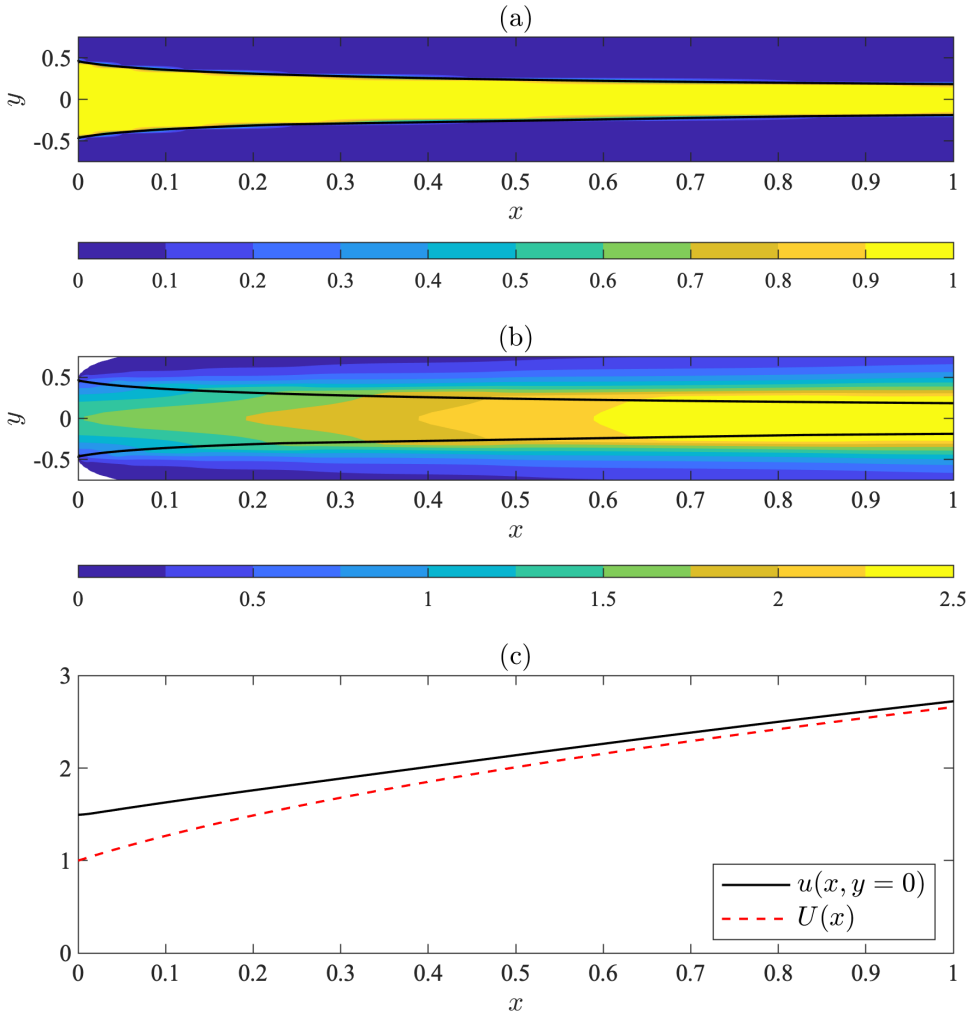

FIG. 3. Two-dimensional curtain flow steady solution: volume fraction C (a) and streamwise velocity component u (b) contours; u distribution on the symmetry axis (black continuous curve) compared with the Torricelli's model (red dashed curve) (c). The curtain-ambient interface is highlighted by a black curve in panels (a) and (b). Here, We $= 2.5$.

a rectangle of area $L^\star \times H_i^\star$ at $t = 0$. Inflow boundary conditions are prescribed at the inlet: at the curtain slot exit section ($-1/2 < y < 1/2$, where $y = y^\star/H_i^\star$), they read as

$$u = \begin{cases} \frac{3}{2}(1 - 4y^2), & t \leqslant t_{\text{steady}} \\ \frac{3}{2}(1 - 4y^2) + u'_f(t), & t > t_{\text{steady}}, \end{cases} \tag{16a}$$

$$v = 0, \tag{16b}$$

$$C = 1, \tag{16c}$$

while the values $u = v = C = 0$ are enforced for $|y| > 1/2$. Note that the streamwise velocity boundary condition, Eq. (16a), is the sum of a steady contribution, corresponding to a fully developed parabolic velocity profile, and an unsteady perturbation $u'_f(t)$. The latter term represents the harmonic forcing [previously defined by Eq. (13)] exciting the curtain varicose dynamics after

TABLE I. Physical quantities involved in the problem, including values corresponding to the two-dimensional steady solutions reported in Fig. 3.

Name	Variable	Value	Unit
Gas density	ρ_a	9.97	$\mathrm{kg\,m^{-3}}$
Liquid density	ρ_l	997	$\mathrm{kg\,m^{-3}}$
Gas viscosity	μ_a	1.84×10^{-5}	$\mathrm{kg\,m^{-1}\,s^{-1}}$
Liquid viscosity	μ_l	8.90×10^{-4}	$\mathrm{kg\,m^{-1}\,s^{-1}}$
Gravity acceleration	g	9.81	$\mathrm{ms^{-2}}$
Inlet liquid mean velocity	$U_i^\star$	0.49	$\mathrm{ms^{-1}}$
Inlet sheet thickness	$H_i^\star$	1.5×10^{-3}	m
Sheet length	$L^\star$	75×10^{-3}	m
Surface tension coefficient	σ	72.5×10^{-3}	$\mathrm{Nm^{-1}}$

the steady base flow solution is achieved, for which a computational time equal to $t_{\mathrm{steady}} \approx 1.5$ is required. A standard free-outflow boundary condition is enforced at the outlet, namely, $p = \partial u/\partial x = \partial v/\partial x = \partial C/\partial x = 0$, while homogeneous Neumann boundary conditions for all variables are enforced on the remaining sides of the domain.

A quadtree-structured grid is employed in the computations, which is characterized by a maximum level of refinement $\mathrm{LoR} = 10$ in a rectangular region containing the entire liquid sheet, and by a dynamical refinement of the cells elsewhere in the domain according to user-defined adaptation criteria (van Hooft *et al.* [30]). In particular, the refinement of a generic grid cell is performed at each iteration reducing by one and then increasing again its grid level, resulting in a down- and up-sampling of the stored scalar fields. Therefore, the error $\chi = ||\phi - \phi^+||$ between the original (ϕ) and the up-sampled (ϕ^+) fields can be estimated; the cell is refined if $\chi > \beta$ and coarsened if $\chi < \beta$, where β is the error threshold of the specific scalar field. For all simulations reported herein, the value $\beta = 1.0 \times 10^{-4}$ has been prescribed for both the velocity components and the volume fraction field. The maximum LoR employed here gives a minimum cell size equal to $\Delta x^\star = 0.05 H_i^\star$, which corresponds to 20 grid cells within $H_i^\star$.

A typical two-dimensional steady base flow obtained by means of the procedure described above is shown in Figs. 3(a) and 3(b) in terms of volume fraction $C(x, y)$ and streamwise velocity component $u(x, y)$ contours, respectively, while in Fig. 3(c) the axial velocity distribution $u(x, y = 0)$ is compared with the Torricelli's model theoretical solution [Eq. (11)]. Values of the inviscid governing parameters (We, Fr, r_ρ, and ε) are the same as those specified in previous Sec. II A. Moreover, since recent studies have shown that varicose modes can arise in sinuously forced liquid curtains only in the high Reynolds number Re limit (Della Pia *et al.* [20]), the volume-of-fluid results reported in this work have been obtained in almost inviscid conditions, namely, for $\mathrm{Re} = \rho_l U_i^\star H_i^\star/(2\mu_l) = O(10^2)$. The analysis of Fig. 3 shows that, as expected, the two-dimensional curtain shape becomes thinner by moving downstream along x [panel (a)], while the liquid flow correspondingly accelerates by gravity [panel (b)]. The small white regions around the left corners of Fig. 3(b) represent negative values of the streamwise velocity in the ambient phase, which highlight a phenomenon of gas entrainment. Moreover, note that the parabolic velocity profile enforced at $x = 0$ progressively relaxes towards a uniform distribution (i.e., constant throughout the curtain thickness) as x increases, which determines the convergence of the axial velocity (black continuous curve) to the Torricelli's one-dimensional theoretical prediction (red dashed curve) by moving downstream along the curtain, as shown in Fig. 3(c).

The physical quantities and the corresponding dimensionless parameters involved in the two-dimensional numerical simulations of the steady curtain flow are summarized in Tables I and II, respectively. The effect of frequency f and amplitude A_u of the harmonic forcing superposed to the base flow for different Weber number We values will be investigated in Sec. III, as regards the simplified 1D linear model, and in Sec. IV, via the 2D VOF simulations.

TABLE II. Dimensionless parameters corresponding to the physical quantities listed in Table I.

Name	Relation	Value
Gas-to-liquid density ratio	$r_\rho = \rho_a/\rho_l$	0.01
Gas-to-liquid viscosity ratio	$r_\mu = \mu_a/\mu_l$	0.02
Sheet slenderness ratio	$\varepsilon = H_i^\star/L^\star$	0.02
Reynolds number	$\mathrm{Re} = \rho_l U_i^\star H_i^\star/(2\mu_l)$	420
Froude number	$\mathrm{Fr} = U_i^{\star 2}/(gL^\star)$	0.33
Weber number	$\mathrm{We} = \rho_l U_i^{\star 2} H_i^\star/(2\sigma)$	2.5

III. FREQUENCY RESPONSE OF 1D VARICOSE DYNAMICS

A. Resonance conditions

The forcing frequency f effect on the one-dimensional curtain flow stationary (i.e., long-time) solution obtained for Weber number $\mathrm{We} = 2.5$ and forcing velocity amplitude $A_u = 0.1$ is first considered; results are reported in Fig. 4. In particular, Fig. 4(a) shows the curtain perturbation thickness spatial distribution $h'(x)$ for three significant values of the forcing frequency, namely, $f = 0.76$ (black curve), $f = 5.34$ (red curve), and $f = 11.43$ (blue curve), while the complete frequency response (i.e., the oscillations amplitude) is reported in Fig. 4(b) as a function of f, for a broad range of forcing frequency values [$f \in [0.15, 15]$]. Note that the function $A_h(f)$ has been scaled with respect to its maximum value $A_{h,\max} = 0.21$.

The nonparallelism of the base flow $U(x)$ due to the gravitational acceleration [see Eq. (11)] determines a spatial variation of the wavelength $\lambda = \lambda^\star/L^\star$ of the curtain thickness perturbation $h'(x)$, which increases by moving downstream along the curtain [$\lambda(x) = U(x)/f$], as shown in Fig. 4(a). By considering the average value of the base flow $\bar{U} = 1.96$ as a reference velocity, one can estimate the average wavelength $\bar{\lambda} = \bar{U}/f$ corresponding to each case. It is thus obtained that $\bar{\lambda} = 2.57$, 0.37, and 0.17 for $f = 0.76$, 5.34, and 11.43, respectively, which well represents the distance between two consecutive peaks of the $h'(x)$ distribution [see, in particular, red and blue

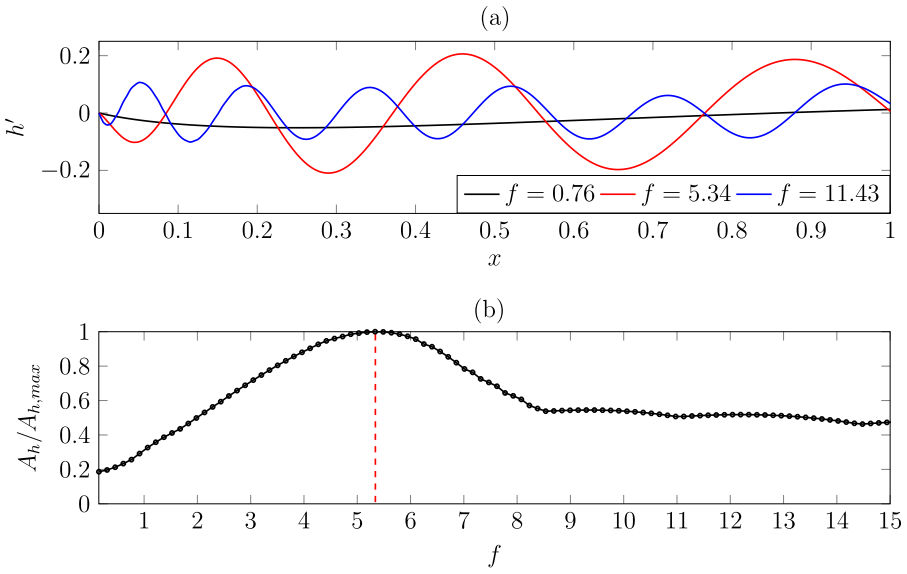

FIG. 4. Forcing frequency f effect on the curtain perturbation thickness spatial distribution $h'(x)$ (a) and on its maximum temporal oscillations amplitude A_h scaled with respect to the value $A_{h,\max} = 0.21$ (b). The red dashed line in (b) denotes the peak frequency $f_{\max} = 5.34$. Here, $\mathrm{We} = 2.5$ and $A_u = 0.1$.

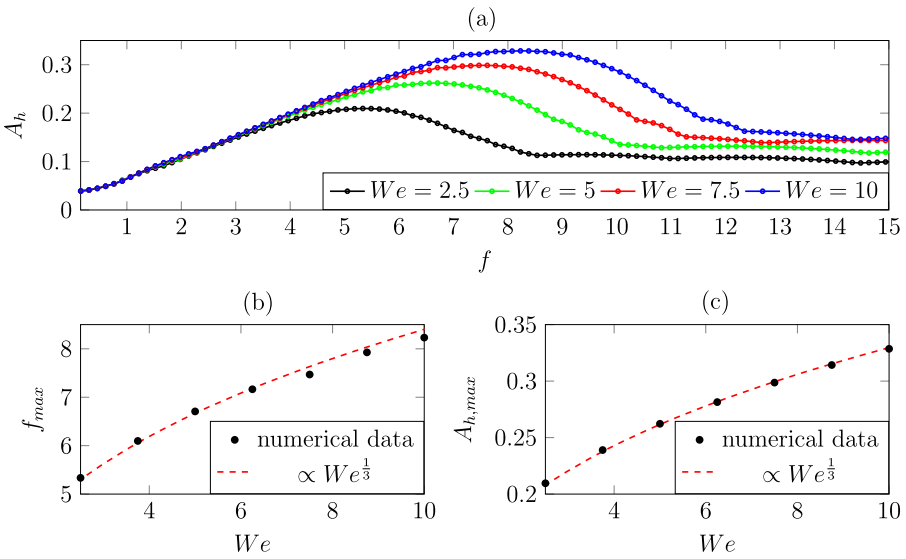

FIG. 5. Frequency response in terms of curtain perturbation thickness A_h as a function of the forcing frequency f (a); peak frequency $f_{\max}$ (b) and corresponding amplitude $A_{h,\max}$ (c) variations with the Weber number We. Here, the forcing amplitude is $A_u = 0.1$.

curves in Fig. 4(a), for which $\bar{\lambda} < 1$]. Moreover, the analysis of Fig. 4(b) reveals that the oscillation amplitude reaches a maximum value equal to $A_{h,\max} = 0.21$ at the forcing frequency $f = 5.34$. Therefore, as a significant result of the present investigation, it is found that the value $f = 5.34$ represents the resonance (and thus the natural) frequency of the flow system for We $= 2.5$, being the trend $A_h(f)$ peaked at $f_{\max} = 5.34$ [red dashed line in Fig. 4(b)].

The varicose oscillatory dynamics of the forced flow is further investigated in Fig. 5, where the Weber number effect on the whole frequency response $A_h(f)$ [panel (a)], the resonance frequency $f_{\max}$ [panel (b)], and the corresponding amplitude $A_{h,\max}$ [panel (c)] are reported in the range We $\in [1.25, 10]$. Note that the Weber number variation is achieved by varying the surface tension coefficient σ. As a valuable result of the present analysis, Figs. 5(b) and 5(c) show that both the resonance frequency $f_{\max}$ and the corresponding maximum amplitude $A_{h,\max}$ exhibit an increasing trend with the Weber number, both following the scaling law $\propto \mathrm{We}^{1/3}$. As a consequence, the average wavelength in resonance conditions scales as $\bar{\lambda}_{\max} \propto \mathrm{We}^{-1/3}$. Theoretical insights on these scaling laws are provided in following Sec. III B.

It is interesting to highlight that results found in this section qualitatively resemble the findings by Le Dizés and Villermaux [34] regarding the destabilization mechanisms of a round (axisymmetric) gravitational viscous liquid jet subjected to noise perturbations, which are distributed along the entire jet length. In particular, these authors theoretically studied the interplay between the instability growth of perturbations and the jet thinning and longitudinal stretching, finding an increasing (decreasing) trend of the most dangerous frequency (wavelength) in the case of a water jet in incipient breakup conditions (see Fig. 9 of Le Dizés and Villermaux [34]). However, it is important to note that, while capillary forces play the well-known destabilizing role for round gravitational liquid jets, in the present planar configuration we found a stabilizing effect of surface tension on the curtain dynamics induced by varicose perturbations. This is discussed in more detail in Sec. IV.

B. Scaling laws of $f_{\max}$ and $A_{h,\max}$ with We number: Theoretical insights

To provide a theoretical justification of the scaling laws reported in Sec. III A for the frequency and amplitude of the stationary (i.e., long-time) varicose oscillations in resonance conditions, one

can reconsider the governing system of Eqs. (7) and (8) under two simplifying assumptions: absence of external gaseous ambient ($r_\rho = 0$) and spatially invariant base flow [$U(x) = \bar{U}$], with $\bar{U}$ being the averaged velocity along the entire curtain length. The simplified system reads as

$$\frac{\partial h'}{\partial t} + \bar{U}\frac{\partial h'}{\partial x} = -\frac{\varepsilon}{\bar{U}}\frac{\partial u'}{\partial x}, \tag{17}$$

$$\frac{\partial u'}{\partial t} + \bar{U}\frac{\partial u'}{\partial x} = \frac{\varepsilon}{4\mathrm{We}}\frac{\partial^3 h'}{\partial x^3}. \tag{18}$$

The common term $\frac{\partial u'}{\partial x}$ can be eliminated from the equations and the system is rearranged into a single partial differential equation, namely,

$$\frac{\partial h'}{\partial t} + \bar{U}\frac{\partial h'}{\partial x} + \frac{\varepsilon^2}{4\bar{U}^2\mathrm{We}}\frac{\partial^3 h'}{\partial x^3} = \frac{\varepsilon}{\bar{U}^2}\frac{\partial u'}{\partial t}. \tag{19}$$

Based on Eq. (19) the evolution of the curtain thickness perturbation $h'(x,t)$ is interpreted as an advection dynamics subjected to a *reaction* term due to the surface tension (which scales with $1/\mathrm{We}$), and *forced* by the (time derivative of) streamwise velocity perturbation $u'(x,t)$ induced via the inlet boundary condition [see Eq. (13) in Sec. II A]. Moreover, as shown in Secs. II A and III A, the governing system of Eqs. (7) and (8) exhibits long-time traveling wave solutions for both the velocity and the thickness perturbations [see, in particular, Figs. 2 and 4(a)]. Therefore, one can assume the following ansatz for the stationary solutions to Eq. (19) of velocity and thickness perturbations:

$$u'(x,t) = A_u \sin(2\pi f t - kx), \tag{20}$$

$$h'(x,t) = A_h \sin(2\pi f t - kx + \varphi). \tag{21}$$

In Eqs. (20) and (21), f is the temporal forcing frequency of the curtain oscillations, k is the spatial wavenumber of the thickness distribution ($k = 2\pi/\lambda$, where λ is the wavelength), and φ represents the phase shift between the forcing (with amplitude A_u) and the response (with amplitude A_h). Note explicitly that due to the assumptions made, the forcing scales linearly with the frequency.

By substituting Eqs. (20) and (21) into Eq. (19) and rearranging the terms, we obtain

$$2\pi\left(f - \frac{\bar{U}}{\lambda}\right) + \frac{8\pi^3\varepsilon^2}{4\bar{U}^2\mathrm{We}}\frac{1}{\lambda^3} = \frac{A_u}{A_h}\frac{2\pi\varepsilon}{\bar{U}^2}f\frac{\cos(2\pi f t - kx)}{\cos(2\pi f t - kx + \varphi)}. \tag{22}$$

By considering the frequency-wavelength relationship $f = \bar{U}/\lambda$, we can rearrange Eq. (22) as the relationship of the gain between the stationary oscillation amplitude A_h and the forcing amplitude A_u, thus obtaining

$$\frac{A_h}{A_u} \propto \frac{\mathrm{We}}{f^2}. \tag{23}$$

Therefore, the amplification of the curtain thickness results from the competition between advection (forcing frequency) and stiffness (surface tension) effects. The case of very high frequency ($f \to \infty$) corresponds to an infinitely stiff curtain ($\mathrm{We} \to 0$), and this scaling law is retrieved in the numerical data shown in Fig. 6, which depicts gain A_h/A_u asymptotically vanishing for high f values and low We numbers.

Let us consider now the opposite case, namely, $\mathrm{We} \to \infty$ (i.e., absence of surface tension) and/or $f \to 0$ (i.e., low forcing frequency); the solution of Eqs. (17) and (18) in terms of curtain oscillation amplitude scales as $A_h/A_u \propto f$, namely, it is a linear function of the forcing frequency f regardless of the Weber number We (see Fig. 6 for $f \to 0$ and/or for $\mathrm{We} \to \infty$). This is due to the fact that the right-hand side of Eq. (18) becomes negligible, thus giving a simple advection equation for the velocity u'. If we again assume a traveling wave form of the perturbations [Eqs. (20) and (21)], it is easy to verify that the advected signal u', acting as a forcing term on the curtain thickness

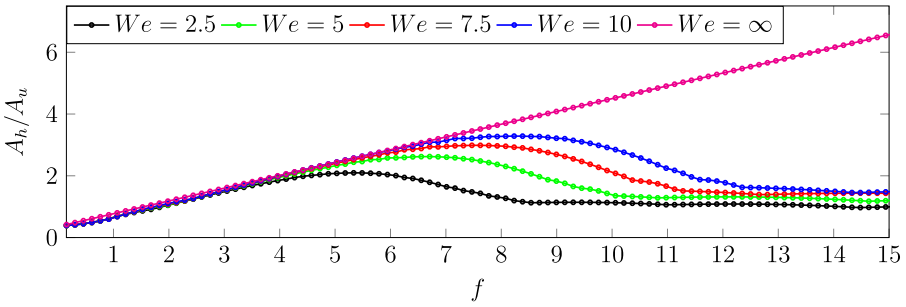

FIG. 6. Gain between the stationary oscillation amplitude A_h and the forcing amplitude A_u as a function of the frequency f by varying the Weber number We.

perturbation [Eq. (17)] via the time derivative $\partial u'/\partial t$, produces an oscillation amplitude A_h varying linearly with f.

Finally, it is interesting to observe that these scaling laws can be further discussed by reconsidering the system of Eqs. (17) and (18) [or, alternatively, Eq. (19)] in two different physical scenarios, namely, for $f^3/\mathrm{We} \ll 1$ and $f^3/\mathrm{We} \gg 1$, with f^3/We scaling the reaction term in the momentum equation (18). Since the amplification $A_h(f)$ linearly increases with f for $f^3/\mathrm{We} \ll 1$, while it monotonically decreases as We/f^2 for $f^3/\mathrm{We} \gg 1$, a maximum $(f_{\max}, A_{h,\max})$, which physically represents the resonance conditions, must exist linking the two regimes. This is found for $f^3/\mathrm{We} = O(1)$, thus retrieving the scaling law of the resonance frequency $f_{\max} \propto \mathrm{We}^{1/3}$ empirically obtained via the numerical simulations presented in previous Sec. III A. By substituting this relation into Eq. (23), the scaling $A_{h,\max} \propto \mathrm{We}^{1/3}$ is also straightforwardly recovered.

IV. VOF SIMULATIONS IN 2D RESONANCE CONDITIONS: THINNING-INDUCED NUMERICAL BREAKUP

The forcing frequency f effect on the two-dimensional curtain flow field obtained with VOF simulations for Weber number $\mathrm{We} = 2.5$ and forcing amplitude $A_u = 0.1$ is reported in Fig. 7. In particular, the streamwise velocity perturbation $u'(x, y)$ contour is shown in panels (a)–(c) for $f = 0.76$, 5.34, and 11.43, respectively, which are the same values as previously considered in Sec. III. The three forcing frequencies are also represented by the vertical dashed lines in panel (d), which reports the fast Fourier transform of the thickness distribution temporal signal $h'(t)$ at the streamwise station $x = 0.5$. Note that each curve in panel (d) is normalized with respect to the overall maximum.

The two-dimensional volume-of-fluid simulations confirm the predictions of the one-dimensional linear analysis: the curtain flow exhibits a resonance behavior at $f = 5.34$ [Fig. 7(d)], for which the varicose oscillations of the curtain reach the maximum amplification. It is also interesting to observe that the varicose displacement of the two curtain-ambient interfaces induces analogous perturbations within the gaseous phase, as can be appreciated by looking at the symmetric (with respect to the axis $y = 0$) velocity contour distributions in Figs. 7(a)–7(c). Note that a curtain-ambient interaction effect via velocity perturbations has also been found by Della Pia *et al.* [20] for a curtain subjected to a normal-to-flow (i.e., sinuous) velocity forcing.

The curtain dynamics in resonance conditions is further investigated in Fig. 8, which shows snapshots of the two-dimensional curtain shapes obtained for $f = f_{\max}$ by varying the inlet forcing amplitude A_u, at the same Weber number values considered in Sec. III. In particular, starting from the value $A_u = 0.1$ so far considered (black curves), the forcing amplitude is increased, and four more cases are investigated: $A_u = 0.15$ (red curves), 0.20 (blue curves), 0.25 (green curves), and 0.30 (magenta curves). The main result arising from the analysis of Fig. 8 is that, in resonance conditions, the curtain breaks up due to the reduction of its thickness induced by the varicose deformation. This

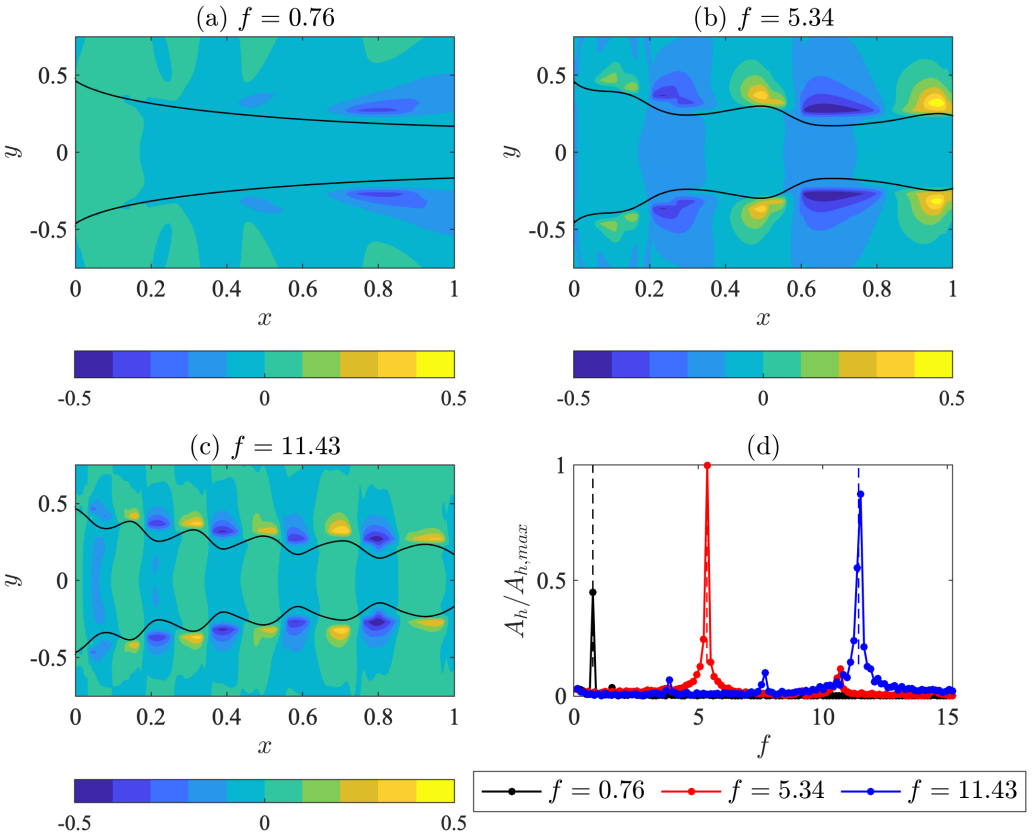

FIG. 7. VOF simulations of two-dimensional curtain flow: streamwise velocity perturbation u' contour (a)–(c) and fast Fourier transform of the thickness perturbation h' (d). Black curves in (a)–(c) denote the curtain-ambient interface. Vertical dashed lines in (d) denote the forcing frequency values: $f = 0.76$ (black); $f = 5.34$ (red); $f = 11.43$ (blue). Here, We $= 2.5$ and $A_u = 0.1$.

thinning-induced numerical breakup results in the formation of an unsteady curtain fragmentation [see, e.g., the magenta curve in Fig. 8(a) for $x \approx 0.8$], which is convected downstream along the curtain by the underlying gravitational base flow and expelled at the domain outlet (not shown in Fig. 8). It is worth pointing out that, once a "thin enough" sheet is created by means of the thinning physical mechanism, one may reasonably assume that the curtain will break due to short-range forces. On the other hand, we recall explicitly that such forces (or other nonequilibrium effects) are of course not included in the Navier-Stokes model here employed.

Interestingly, for each Weber number value considered, the reduction of curtain thickness induced by the varicose deformation (which leads to numerical breakup) occurs at a specific value of the forcing amplitude, i.e., $A_u = 0.30$, not depending on We. On the other hand, it can be seen that the streamwise station where this thinning occurs moves upstream by increasing the Weber number [e.g., it goes from $x \approx 0.8$ for We $= 2.5$, panel (a), to $x \approx 0.5$ for We $= 10$, panel (d)], i.e., it shifts downstream by considering progressively higher values of the surface tension coefficient, thus "spatially delaying" the breakup. In this respect, surface tension is found to play a stabilizing role on the varicose oscillations of the gravitational curtain. Note that a stabilizing effect of surface tension on the convective instability of unconfined planar liquid jets was also found by Turner *et al.* [36] by means of spatiotemporal stability analysis.

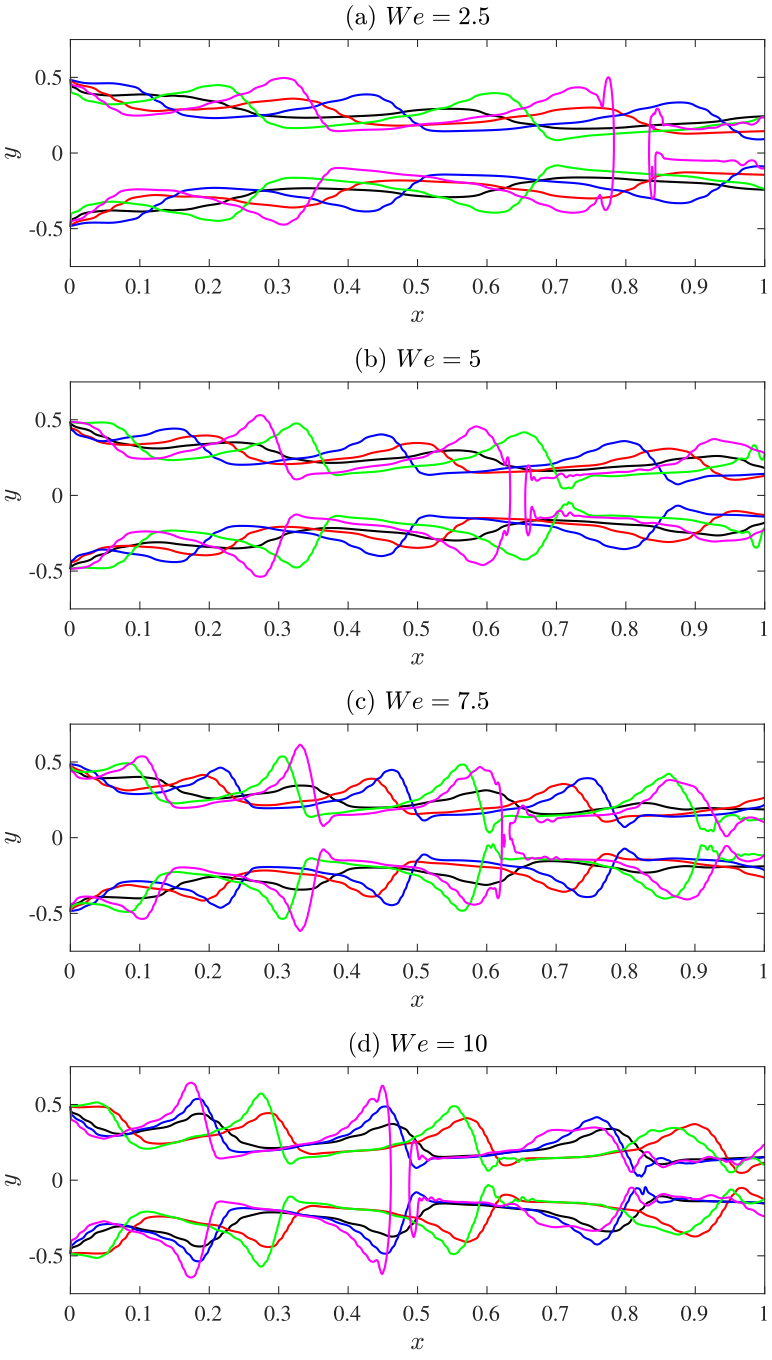

FIG. 8. Curtain shape in resonance conditions for different values of the Weber number We by increasing the forcing amplitude A_u: 0.1 (black); 0.15 (red); 0.2 (blue); 0.25 (green); 0.3 (magenta).

The thinning-induced numerical breakup of liquid curtain found here significantly resembles the experimental findings by Lhuissier *et al.* [37]. These authors studied the response of a steady free-falling liquid sheet to localized varicose perturbations, which were imposed at fixed streamwise

TABLE III. Resonance frequency $f_{\max}$ as a function of the Weber number We. The corresponding average wavelength $\bar{\lambda}_{\max}$ and amplitude $A_{h,\max}$ of the varicose oscillations are also reported. Here, the forcing amplitude is $A_u = 0.1$.

We	2.5	5	7.5	10
$f_{\max}$	5.34	6.71	7.47	8.23
$\bar{\lambda}_{\max}$	0.37	0.29	0.26	0.24
$A_{h,\max}$	0.21	0.26	0.30	0.33

stations along the curtain. The perturbations were generated by blowing the liquid curtain by means of two air jets symmetrically located with respect to the curtain frontal plane, and thus able to introduce a varicose perturbation in the form of a local curtain thinning with controlled amplitude. For all the liquid flow rates investigated, Lhuissier *et al.* [37] found that the varicose thinning of the curtain determined the formation of a steady hole downstream from the perturbation location. Although a quantitative comparison between present results and those of Lhuissier *et al.* [37] is made unfeasible by the different flow-rate ranges investigated (here, the flow rate is $Q^\star = U_i^\star H_i^\star = 7.35$ cm^2/s, while in Lhuissier *et al.* [37] it is $Q^\star \in [0.6, 4.5]$ cm^2/s), the physical mechanism determining the hole formation outlined by Lhuissier *et al.* [37] is the same which causes the 2D curtain (numerical) breakup in the present work, namely, a thinning of the curtain induced by the varicose perturbations. However, it is worth pointing out that Lhuissier *et al.* [37] considered *steady* varicose perturbations generated by continuously blowing the curtain, thus determining the formation of a steady hole in the liquid flow. On the contrary, we have examined here the response of the curtain to *time-varying* (harmonic) perturbations, which results in the formation of an unsteady (2D) fragmentation advected downstream by the underlying gravitational base flow.

The values of the resonance frequency $f_{\max}$ and the corresponding average wavelength $\bar{\lambda}_{\max}$ and amplitude $A_{h,\max}$ of the varicose oscillations as a function of the Weber number We are summarized in Table III, for a forcing amplitude $A_u = 0.1$. As already outlined in Sec. III, it is found that $f_{\max}$ and $A_{h,\max}$ increase with We, both following the scaling law $\propto$We$^{1/3}$, while $\bar{\lambda}_{\max}$ decreases as We$^{-1/3}$. In the same way as the natural frequency, the average wavelength $\bar{\lambda}_{\max}$ predicted by the one-dimensional linear model is also well retrieved in the two-dimensional volume-of-fluid simulations. This can be appreciated in Fig. 9, which shows the curtain shapes obtained using the two methodologies when breakup conditions are approached. Note that the 1D linear shape has been

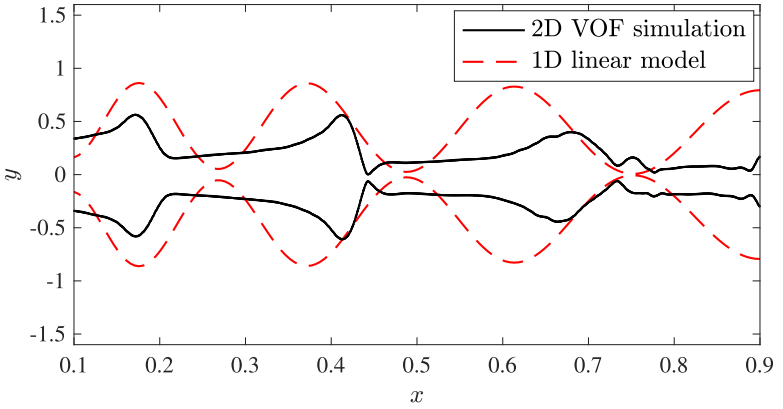

FIG. 9. Curtain shape induced by the varicose forcing as predicted by the one-dimensional linear model (red dashed curve) and the two-dimensional volume-of-fluid simulation (black curve) approaching breakup conditions. Here, We $= 10$, $f = 8.23$, and $A_u = 0.25$.

obtained by superposing to the base flow thickness distribution $H = 1/U$ [see Eq. (11) in Sec. II A] the perturbation quantity $h'(x,t)$ obtained for We $= 10$, $f = 8.23$, and $A_u = 0.25$. As shown in Fig. 9, the 1D linear model correctly predicts the wavelength of the varicose perturbation dynamics, as well as the thinning of the curtain leading to breakup, while of course it is not able to reproduce the nonlinear saturated shape characterizing the curtain in incipient breakup conditions.

Finally, it is interesting to observe that the 2D nonlinear shapes shown in Figs. 8 and 9 qualitatively agree with the typical experimental shapes of axisymmetric liquid jets accelerated by faster coaxial gaseous streams, as those reported, for example, in Fig. 38 of Eggers and Villermaux [38].

V. CONCLUSIONS

The varicose dynamics of a forced gravitational liquid sheet (curtain) issuing into a quiescent gaseous ambient has been numerically studied. The investigation has been performed in supercritical regime, namely, for Weber number We > 1. Two methodologies have been employed: a simplified one-dimensional linear model, and two-dimensional VOF simulations. Employing harmonic forcing perturbations of the streamwise velocity applied at the inlet section, the varicose dynamics of the curtain has been excited and characterized by varying the forcing frequency f and amplitude A_u of the perturbations, for different values of We.

As a first significant result, the one-dimensional linear analysis has shown that the curtain oscillations amplitude reaches a maximum for a certain forcing frequency $f = f_{\max}$. In other terms, it has been found that the flow manifests a resonance behavior, with the natural oscillation frequency $f_{\max}$ and corresponding amplitude $A_{h,\max}$ both scaling as $\mathrm{We}^{1/3}$, while the average wavelength $\bar{\lambda}_{\max}$ scales as $\mathrm{We}^{-1/3}$. These scaling laws have been fully recovered by theoretical insights. The two-dimensional VOF simulations have confirmed the one-dimensional model predictions of the flow natural frequency, as well as of the wavelength in resonance conditions.

It has been also found that the curtain breaks up by increasing the forcing amplitude A_u, exhibiting a nonlinear saturated shape in incipient breakup conditions, recalling that of axisymmetric liquid jets sheared by faster coaxial gaseous streams. The rupture is determined by a reduction of the curtain thickness induced by the varicose deformation, and it occurs at a specific value of the forcing amplitude, which does not depend on the Weber number. It has been explicitly stressed that the nature of this breakup is numerical because the relevant short-range forces are not included in the Navier-Stokes model here employed. The streamwise station where the curtain thinning occurs moves upstream by increasing We, i.e., it shifts downstream by increasing the surface tension coefficient, thus "spatially delaying" the numerical breakup. In this respect, the surface tension is found to play a stabilizing role on the varicose oscillations of the curtain.

The present work constitutes, together with previous investigations in the literature of the sinuous dynamics of liquid curtains, a further step towards deriving a weakly nonlinear mathematical model accounting for the coupling between sinuous and varicose modes in such flow configurations.

The data that support the findings of this study are available from the Contact author upon reasonable request.

ACKNOWLEDGMENTS

The two-dimensional numerical simulations included in the present work were performed on resources granted by CINECA under the ISCRA-C project HONOUR-2. The authors would like to acknowledge the anonymous referees for their valuable comments, especially for inspiring the 1D theoretical scaling law analysis reported in Sec. III B and clarifying the numerical nature of the 2D curtain breakup shown in Sec. IV.

The authors report no conflict of interest.

[1] S. P. Lin, Stability of a viscous liquid curtain, J. Fluid Mech. **104**, 111 (1981).
[2] L. Rayleigh, *The theory of sound* (Macmillan and Co., London, 1877).
[3] G. Taylor, The dynamics of thin sheets of fluid. III. Disintegration of fluid sheets, Proc. R. Soc. London Ser. A **253**, 313 (1959).
[4] H. B. Squire, Investigation of the instability of a moving liquid film, Br. J. Appl. Phys. **4**, 167 (1953).
[5] D. R. Brown, A study of the behaviour of a thin sheet of moving liquid, J. Fluid Mech. **10**, 297 (1961).
[6] J. Roche, N. Le Grand, P. Brunet, L. Lebon, and L. Limat, Perturbations on a liquid curtain near break-up: Wakes and free edges, Phys. Fluids **18**, 082101 (2006).
[7] N. Le Grand-Piteira, P. Brunet, L. Lebon, and L. Limat, Propagating wave pattern on a falling liquid curtain, Phys. Rev. E **74**, 026305 (2006).
[8] A. Bers, Space–time evolution of plasma instabilities—absolute and convective(North-Holland, Netherlands, 1983), http://inis.iaea.org/search/search.aspx?orig_q=RN:15068895.
[9] S. P. Lin, Z. W. Lian, and B. J. Creighton, Absolute and convective instability of a liquid sheet, J. Fluid Mech. **220**, 673 (1990).
[10] L. De Luca and M. Costa, Instability of a spatially developing liquid sheet, J. Fluid Mech. **331**, 127 (1997).
[11] N. S. Barlow, B. T. Helenbrook, and S. P. Lin, Transience to instability in a liquid sheet, J. Fluid Mech. **666**, 358 (2011).
[12] A. Della Pia, A. Colanera, M. Chiatto, and L. de Luca, Energy insights into the unsteady dynamics of a viscous gravitational liquid sheet, Phys. Fluids **33**, 092118 (2021).
[13] A. Colanera, A. Della Pia, and M. Chiatto, Data-driven global stability of vertical planar liquid jets by DMD on random perturbations, Phys. Fluids **34**, 122101 (2022).
[14] B. Torsey, S. J. Weinstein, D. Ross, and N. Barlow, The effect of pressure fluctuations on the shapes of thinning liquid curtains, J. Fluid Mech. **910**, A38 (2021).
[15] M. Chiatto and A. Della Pia, Natural frequency discontinuity of vertical liquid sheet flows at transcritical threshold, J. Fluid Mech. **945**, A32 (2022).
[16] M. Girfoglio, F. De Rosa, G. Coppola, and L. de Luca, Unsteady critical liquid sheet flows, J. Fluid Mech. **821**, 219 (2017).
[17] H. Bodhanwalla, C. Anghan, and J. Banerjee, The effect of one-sided confinement on nappe oscillations in free falling liquid sheet, Phys. Fluids **34**, 124107 (2022).
[18] A. Della Pia, A. Colanera, and M. Chiatto, Surface tension-induced instability in spatially developing subcritical liquid curtains, Phys. Fluids **34**, 042122 (2022).
[19] S. J. Weinstein and K. J. Ruschak, Coating flows, Annu. Rev. Fluid Mech. **36**, 29 (2004).
[20] A. Della Pia, M. Chiatto, and L. de Luca, Receptivity to forcing disturbances in subcritical liquid sheet flows, Phys. Fluids **33**, 032113 (2021).
[21] A. Colanera, A. Della Pia, M. Chiatto, L. de Luca, and F. Grasso, Modal decomposition analysis of unsteady viscous liquid sheet flows, Phys. Fluids **33**, 092117 (2021).
[22] A. Kornecki, E. H. Dowell, and J. O'Brien, On the aeroelastic instability of two-dimensional panels in uniform incompressible flow, J. Sound Vib. **47**, 163 (1976).
[23] F. De Rosa, Dinamiche instazionarie ed instabilitá lineare globale di getti liquidi, Ph.D. thesis, Universitá di Napoli Federico II, 2013, http://www.fedoa.unina.it/9459.
[24] D. S. Finnicum, S. J. Weinstein, and K. J. Rushak, The effect of applied pressure on the shape of a two-dimensional liquid curtain falling under the influence of gravity, J. Fluid Mech. **255**, 647 (1993).
[25] S. J. Weinstein, A. Clarke, A. Moon, and E. Simister, Time-dependent equations governing the shape of a two-dimensional liquid curtain, part 1: Theory, Phys. Fluids **9**, 3625 (1997).
[26] R. Scardovelli and S. Zaleski, Direct numerical simulation of free-surface and interfacial flow, Annu. Rev. Fluid Mech. **31**, 567 (1999).
[27] S. Popinet, Gerris: A tree-based adaptive solver for the incompressible Euler equations in complex geometries, J. Comput. Phys. **190**, 572 (2003).
[28] S. Schmidt and K. Oberleithner, Instability of forced planar liquid jets: Mean field analysis and nonlinear simulation, J. Fluid Mech. **883**, A7 (2020).
[29] S. Schmidt, O. Tammisola, L. Lesshafft, and K. Oberleithner, Global stability and nonlinear dynamics of wake flows with a two-fluid interface, J. Fluid Mech. **915**, A96 (2021).

[30] J. A. van Hooft, S. Popinet, C. C. van Heerwaarden, S. J. A. van der Linden, S. R. de Roode, and B. J. H. van de Wiel, Towards adaptive grids for atmospheric boundary-layer simulations, Boundary Layer Meteorol. **167**, 421 (2018).
[31] G. G. Agbaglah, Breakup of thin liquid sheets through hole-hole and hole-rim merging, J. Fluid Mech. **911**, A23 (2021).
[32] M. M. Francois, S. J. Cummins, E. D. Dendy, D. B. Kothe, J. M. Sicilian, and M. W. Williams, A balanced-force algorithm for continuous and sharp interfacial surface tension models within a volume tracking framework, J. Comput. Phys. **213**, 141 (2006).
[33] S. Popinet, An accurate adaptive solver for surface-tension-driven interfacial flows, J. Comput. Phys. **228**, 5838 (2009).
[34] S. Le Dizés and E. Villermaux, Capillary jet breakup by noise amplification, J. Fluid Mech. **810**, 281 (2016).
[35] http://basilisk.fr.
[36] M. R. Turner, J. J. Healey, S. S. Sazhin, and R. Piazzesi, Stability analysis and breakup length calculations for steady planar liquid jets, J. Fluid Mech. **668**, 384 (2011).
[37] H. Lhuissier, P. Brunet, and S. Dorbolo, Blowing a liquid curtain, J. Fluid Mech. **795**, 784 (2016).
[38] J. Eggers and E. Villermaux, Physics of liquid jets, Rep. Prog. Phys. **71**, 036601 (2008).